Drop Shapes and Fall Speeds in Rain: Two Contrasting Examples

M. THURAI AND V. N. BRINGI

Department of Electrical and Computer Engineering, Colorado State University, Fort Collins, Colorado

W. A. PETERSEN

NASA Wallops Flight Facility, Wallops Island, Virginia

P. N. GATLIN

NASA Marshall Space Flight Center, Huntsville, Alabama

(Manuscript received 29 March 2012, in final form 22 May 2013)

ABSTRACT

Two rain events are analyzed using two collocated 2D-video disdrometers (2DVD) and a C-band polarimetric radar at 15-km distance. Both events had moderate-to-intense rainfall rates, but the second event had an embedded convective line. For the first event, the fall speed distribution for a given drop diameter interval showed a narrow and symmetric distribution with a mode at the expected value; the second event produced a wider distribution with a significant skewness toward lower fall speeds. The ''slower'' drops in the second event were detected while the convective line was directly over the 2DVD site. Drop shape information from the two 2DVD instruments showed that, during the passage of the convection line, around 30%–40% of the drops did not have an axis of rotational symmetry, whereas for event 1, it was only 5%. The implications are that for event 1 the dominant mode of drop oscillation is the axisymmetric mode, and that within the convective line of event 2 other fundamental modes were frequent. The radar data for the second event were analyzed in terms of the self-consistency among the radar-measured quantities. The K_{dp}/Z_h versus Z_{dr} variations within the line convection were not consistent with the corresponding variation determined from the scattering calculations using the measured 1-min drop size distributions and using the ''reference'' drop shapes. Also found were low ρ_{hv} regions within the line convection that were considerably lower than the scattering calculations. These findings are consistent with the asymmetric oscillation modes inferred from the 2DVD measurements for event 2 (probably collision induced) within the convective line.

1. Introduction

The fall speed of raindrops as a function of drop diameter is important in cloud physics and forms a fundamental basis for radar-based estimation of rain rate. The laboratory data of Gunn and Kinzer (1949; henceforth GK) for fall speed (of water drops in still air), and the fits to their data, continue to be widely recognized as the ''standard'' against which to compare measurements made with more modern optical techniques (e.g., Löffler-Mang and Joss 2000; Barthazy et al. 2004; Schönhuber et al. 2008). These latter optical disdrometers are capable of measuring both drop shapes and their fall speeds, which in turn allows for determining if there is any coupling between the two, especially in moderate-to-intense rain rates where drop oscillations may be expected to significantly affect the drag force relative to spherical drops in still air. Additionally, the distribution of fall speeds for a given diameter is also relevant. One might expect a Gaussian distribution centered on the GK values because of turbulence, but significant skewness might result as reported herein for larger drops in intense rainfall (under certain conditions such as embedded line convection). We note that an opposite skewness (i.e., toward higher fall speeds) for tiny drops (diameter D near 0.4 mm) was found by Montero-Martinez et al. (2009) related to drop breakup. Since a theoretical treatment is lacking at present, we must rely on high-quality (i.e., well calibrated and accurate) disdrometers

Corresponding author address: M. Thurai, Dept. of Electrical and Computer Engineering, Colorado State University, Fort Collins, CO 80523-1373.
E-mail: merhala@engr.colostate.edu

DOI: 10.1175/JAMC-D-12-085.1

© 2013 American Meteorological Society

capable of simultaneously measuring drop volume, fall speed, shape, and orientation angles in natural rainfall. The 2D video disdrometer (2DVD) is, to the best of our knowledge, the only instrument that is capable of providing such data (Schönhuber et al. 2008) for moderate-to-large-sized drops ($D \geq 1.5$ mm). For example, the 80-m fall experiment involving artificially generated drops up to 9.5 mm in (equivolume) diameter showed excellent agreement of fall speeds with that of GK up to 6 mm (Thurai and Bringi 2005). Beyond 7 mm a decreasing trend in fall speed was found, perhaps because of an increase in drag due to large drop distortion (i.e., related to large-amplitude oscillations).

Regarding drop shapes for D in the range 2.5–7 mm, the "average" shapes determined from a large sample of individual "snapshots" made with the 2DVD were in excellent agreement with wind-tunnel-derived "dynamic" equilibrium shapes determined by high-speed imaging of individual drops as they go through many cycles of oscillation (Szakáll et al. 2009; Thurai et al. 2009b). From a frequency analysis of the time series of axis ratios, Szakáll et al. found that the dominant mode of oscillation (for $D > 2.5$ mm) was the axisymmetric (oblate–prolate) mode, with small-amplitude transverse modes also being mixed in (e.g., Foote 1973; Beard 1984; Feng and Beard 1991). The highly symmetric axis ratio distributions (about the equilibrium value) from the 80-m fall bridge experiment also support, indirectly, the dominance of the axisymmetric mode for $D > 2$ mm (see also Kubesh and Beard 1993). We refer to the review articles of Szakáll et al. (2010) and Beard et al. (2010) and references contained therein for a fuller description of drop shapes and oscillation modes. In brief, Beard and Kubesh (1991) describe the three distinct fundamental frequency oscillation modes: (i) the aforementioned axisymmetric (spherical harmonic $n = 2, m = 0$) mode, (ii) the transverse oscillation ($n = 2, m = 1$) mode, and (iii) the horizontal ($n = 2, m = 2$) mode.

While the recent wind-tunnel and 80-m fall bridge data form a valuable reference regarding fall speeds, shapes, and dominant oscillation modes, data in natural rain are more limited, especially under a wide range of rain rates. In a significant field study using camera-recorded fall streaks and strobe lights to infer drop oscillations and fall speeds (and a disdrometer to measure drop size distributions and rain rates), Tokay and Beard (1996) concluded that persistent oscillations for larger drops ($D > 2.0$ mm or so) "is a consequence of changes in drag that should produce a positive feedback to oscillations of fundamental oblate–prolate mode." High-speed imaging of drop oscillations and fall speeds in one light rain rate (1 mm h^{-1}) event by Testik et al. (2006) showed evidence of multimode oscillations (see Fig. 3 of Testik et al. 2006) for drops in the range 1.5–2 mm, with a small decrease in fall speed (around 10%) from GK. They wrote that the decrease in fall speed is "possibly due to increased drag force induced by large amplitude oscillations." Deviations of axis ratio distributions from the reference 80-m fall bridge data have been observed in one convective rain event in Huntsville, Alabama, during different periods of the storm passage over the 2DVD site (Thurai et al. 2009a). Here the axis ratio distribution for the 3.5-mm-sized drops was found to be wider with positive skewness (toward sphericity) observed during the high-rain-rate period (>50 mm h^{-1}) as opposed to the more "normal" axis ratios during the lower-rain-rate period. The wider distribution and positive skewness during the high-rain-rate period was inferred to be a result of mixed-mode oscillations (axisymmetric mixed with transverse mode; see also Beard 1984). Simultaneous polarimetric radar data, when compared with drop-by-drop scattering simulations from the 2DVD (using measured shapes and orientation angles; see Huang et al. 2008 for the latter), were found to be in good agreement during the different rain-rate periods. Indeed this study highlighted the possibility of "significant" deviations of axis ratios from the usually assumed model in natural rain under certain conditions (e.g., Beard and Chuang 1987; Brandes et al. 2002).

In this paper, we report on an in-depth analysis of two cool season precipitation events that occurred within 7 days of each other in Huntsville: (i) one event conforming to the 80-m fall bridge data regarding drop axis ratios and fall speeds and (ii) the second event showing significant deviations, in particular with regard to fall speeds and drop shapes within one period of the storm passage over the 2DVD site. Measurements were made using two collocated (i.e., a few meters apart) and accurately calibrated 2DVDs as well as a C-band polarimetric radar [Advanced Radar for Meteorological and Operational Research (ARMOR); Petersen et al. 2007] located 15 km from the 2DVD site. The measurements were part of an ongoing long-term campaign.

Our paper is organized as follows. A brief description of the two precipitation events is given in section 2 based on radar reflectivity images and on the embedded convective line that dominated the second event. The 2DVD measurements of fall speeds are discussed in detail in section 3 focusing on the differences between the two events. Section 4 deals exclusively with the second event describing the polarimetric radar data (reflectivity Z_h, differential reflectivity Z_{dr}, and specific differential propagation phase K_{dp}), especially the differences observed within the embedded convective line as opposed to the widespread precipitation surrounding the line. Section 5 discusses our findings by combining the 2DVD data

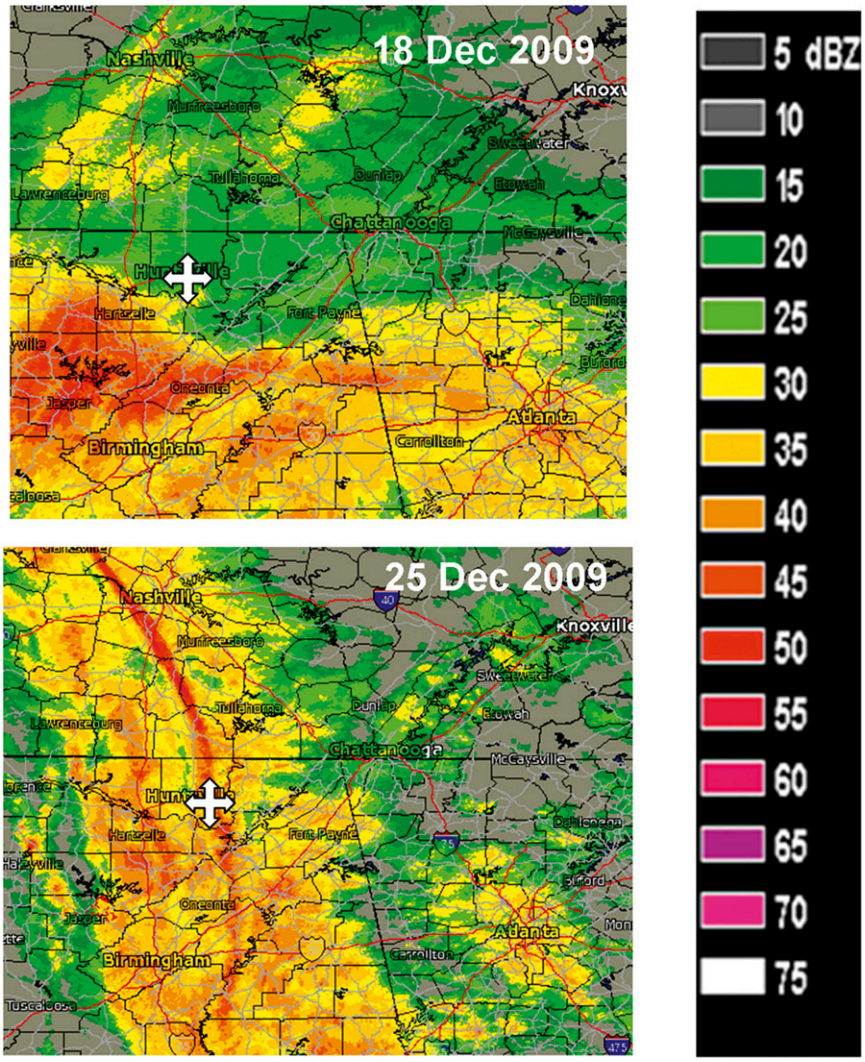

FIG. 1. Composite radar images of the two events considered in this study. The white plus signs show the location of the two 2DVDs in Huntsville. The ARMOR is situated 15 km away in the southwest direction. Note the embedded line convection crossing the 2DVD location in the case of the event on 25 Dec 2009 (event 2).

with the polarimetric radar data, along with prior referenced work. The paper ends with a summary of observations and our inferences related to coupling of the slower fall speeds in event 2 with mixed-mode oscillations.

2. The two events

The two events, which occurred on 18 and 25 December 2009, were of long duration lasting several hours. Figure 1 shows the composite radar images of the two events around the Huntsville area. The white cross in both panels marks the 2DVD location. In both cases, the event had high reflectivities, but for case 2 a well-defined thin line of embedded convection can be seen crossing the Huntsville area. The first event was associated with an overrunning rainfall event from a warm front moving north from the Gulf of Mexico, whereas the second event was associated with a prefrontal rainband similar to that which occurs with cold fronts aloft (Hobbs et al. 1996). Both events had relatively high rainfall accumulations. Table 1 compares the daily totals from the two 2DVD units and from a Geonor rain gauge, also collocated. There appears to be no perceptible bias (less than a few percent) in the rain accumulation estimates. The time series of rain accumulation from the 2DVDs and the Geonor are considered later in the next section when discussing the accuracy of the 2DVD-based fall speed measurements.

TABLE 1. Total rainfall (mm) from the two 2DVDs and from the collocated Geonor rain gauge.

Date	Low-profile 2DVD (SN-16)	Compact 2DVD (SN-25)	Geonor
18 Dec 2009 (event 1)	35.5	>33.2*	34.5
25 Dec 2009 (event 2)	26.2	24.4	25.4

* Some loss of data for several minutes as a result of a minor instrument problem.

In terms of wind speeds at 10-m height, event 1 registered average speeds in the range 2–5 $m\,s^{-1}$ with a maximum of up to 7 $m\,s^{-1}$, whereas event 2 registered average speeds of 8 $m\,s^{-1}$ during the convective line passage, with a maximum of 13 $m\,s^{-1}$.

3. 2DVD measurements

The two units used here are the ''low profile'' and the third-generation compact versions (which are similar in design), as opposed to the ''tall'' unit for which Nešpor et al. (2000) have shown that wind-flow blockage by the instrument can cause local effects over the sensor area in high wind situations. While the wind blockage effects have not been modeled for these low-profile units, they are expected to be very much less than for the tall unit. High horizontal winds will affect the small drops causing the virtual measurement area to be filled only partially (see appendix of Schuur et al. 2001); such partial filling was not observed in either instrument for the two events (see also Godfrey 2002).

The 1-min drop size distribution (DSD) measurements from one of the 2DVD units are shown in Figs. 2a and 2b for the two events. The first event lasted over 18 h, having drops with equivolume diameter D_{eq} up to 4.5–5 mm. The second event, which also had large drops, lasted for over 4 h, but within a 10-min period there were drops as large as D_{eq} of 6 mm. The black (upper) points in Figs. 2a and 2b represent the mass-weighted mean diameter determined from the 1-min DSD and the gray (lower) lines represent the standard deviation of the mass spectrum.

The 2DVD measures the drop fall speed (i.e., the vertical velocity component) for each drop falling within the sensor area, as well as the shape, size, and orientation. Figures 2c and 2d show the measured fall speed versus D_{eq} for the two events. In each case, the orange points represent the mean velocity $\pm$ 1 standard deviation from the low-profile 2DVD and the green points represent those from the compact 2DVD. The dashed curve represents the expected variation based on the equation given in Atlas et al. (1973), which is a fit to the GK data at ground level. The fall velocity measurements for the first event lie close to the expected curve, but the second event shows significantly lower fall speeds, particularly for the larger drops, namely, for $D_{eq} > 3$ mm. Note that fall velocity from the 2DVD is a direct measurement by matching drops from camera A and B; that is, fall velocity is based on the calibrated distance between the two light planes divided by the time required for the same (i.e., matched) drop to ''hit'' the top light plane and then the bottom light plane (Schönhuber et al. 2008). The horizontal drop velocity component does not enter into this calculation.

The distributions of the measured vertical velocity for all the 3-mm drops (to be precise, 3 $\pm$ 0.1 mm) for both events are shown in Fig. 3. The number of drops in this size range was sufficient to derive a probability distribution function–like distribution. While the histograms for larger-sized drops tended to be more ''noisy,'' they also showed negative skewness. For each of the two events, the two instruments show good agreement (thus providing confidence in the accuracy of the 2DVD measurements) but the two events are markedly different from each other. Whereas for event 1, the distributions are narrow and symmetric and have a mode close to the expected fall velocity for D_{eq} = 3 mm (8 $m\,s^{-1}$), the second event shows a wider distribution with a noticeable negative skewness. While both events had different wind conditions, the skewness for the second event (25 December 2009) cannot be explained easily. Note that Huang et al. (2010) have simulated the effect of mismatched drops on the fall speed and equivalent diameter of 3-mm spherical particles. They show that mismatching would preferentially cause positive skewness in the fall speeds, which is opposite to the skewness noted for the second event in Fig. 3. In general, larger-sized drops ($D_{eq} > 1.5$ mm) are much easier to match as compared to tiny ones given the finite instrument resolution (around 0.16 mm) along with their high concentration and near-spherical shapes.

As mentioned earlier, the 2DVD records the contoured information about each individual hydrometeor falling through its sensor area. Each of the drop images also has the corresponding ''time stamp'' recorded and hence it is possible to examine the time series of the drop fall velocities as the event passes over the 2DVD site. Figures 4a and 4b show the fall velocity–time plots from the two instruments for the two events for a 4-h period. For event 1, the fall velocities lie close to the expected value (7.9–8 $m\,s^{-1}$) throughout the 4-h time period, but for event 2, relatively large fall velocity fluctuations occur between 0330 and 0350 UTC, with a significant

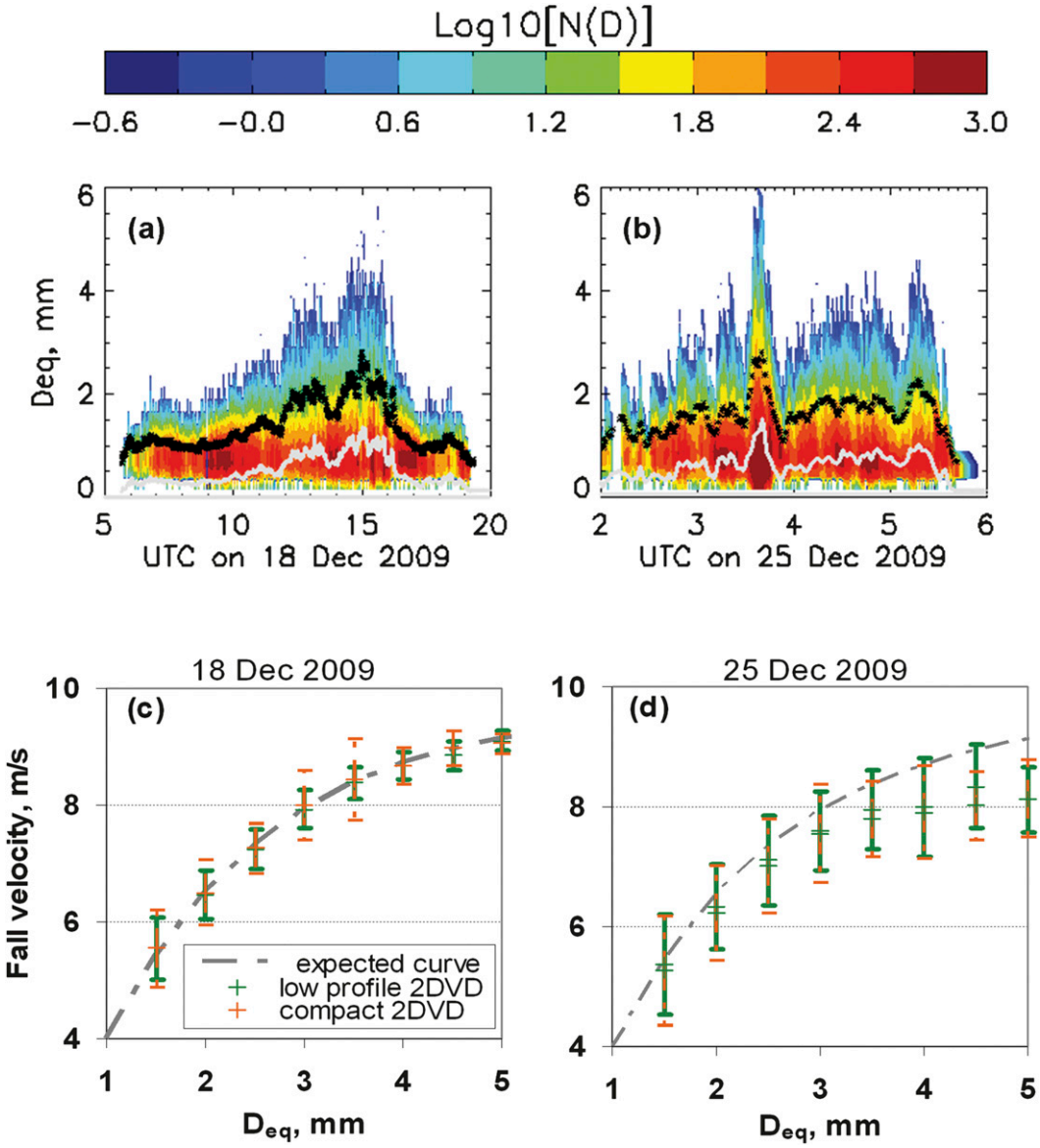

FIG. 2. (a) The 1-min drop size distribution for the first event; (b) as in (a), but for the second event. (c) The measured fall velocity vs equivalent drop diameter for the first event 1; (d) as in (c), but for the second event.

proportion of the drops having lower than the expected velocities.[1] Outside this time range, the 3-mm drop velocities show much less variation and are centered around the expected value (as was the case in the first event). To confirm that there were no instrument problems, in Figs. 4c and 4d we present plots for the second event generated from each of the two instruments. In both sets of measurements, the same behavior was observed. The negative skewness for the second event seen earlier in fall velocity distributions (Fig. 3) arises primarily because of the "slower" 3-mm drops captured between 0330 and 0350 UTC. This is significant, and cannot be dismissed as being due to any instrument "calibration problems." In Fig. 5a we show the 1-min wind speeds at 10-m height (solid line) for the 25 December 2009 event, along with the 3-mm drop fall speeds (plus signs). There is no correlation between fall speed and wind speed. We also show (Fig. 5b) the same figure except zoomed in to cover the time period of the line passage. Again, there is no correlation between wind speeds and 3-mm fall speeds. To reemphasize the

[1] Drops with larger D_{eq} showed similar behavior and are not presented here.

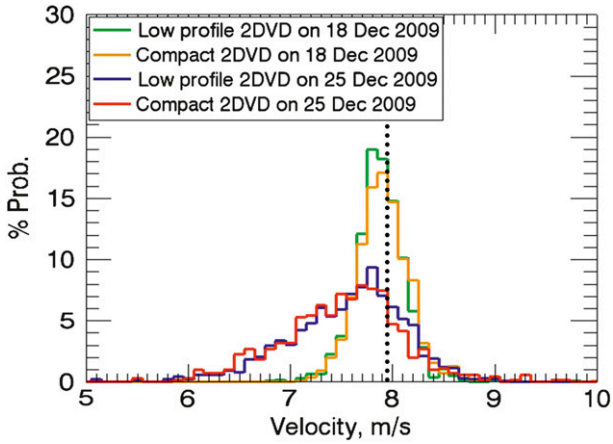

FIG. 3. Distribution of measured fall velocities of all 3-mm drops from the two 2DVD measurements for events 1 and 2. The dotted black vertical line indicates the expected fall velocity for the 3-mm drops in a standard atmosphere.

above point, we show in Fig. 5c the histograms of the 3-mm fall speeds conditioned by wind speeds greater than and less than $7\,\mathrm{m\,s^{-1}}$. There are no systematic differences between the two histograms, confirming no correlation with wind speeds. Note additionally that the wind speed at 30–40 cm above ground level (the height of the 2DVD sensor area) will be much lower than the 10-m wind speeds. We must also reiterate here that fall speed from the 2DVD is based on the time taken for the drop to fall between the two light planes and has nothing to do with the drop's horizontal velocity component. This was shown clearly in Schönhuber et al. (2008, 14–15), and is the basic principle behind having two optical planes with precisely calibrated vertical offset including any small nonparallelism between the two planes. In practice, mismatching of small drops ($D < \sim 0.8$ mm) can cause false "fall speed" estimates, but certainly not for larger drops ($D > \sim 1.5$ mm), which can be easily matched, since the larger drops will have more scan lines and pixels defining them (from each camera) and their number concentrations are considerably less.

The data in Fig. 4 represent the actual fall speed, with no contribution from the wind-induced horizontal component [see Eq. (1) in Schönhuber et al. 2008]. Further, the fall speed is used to calculate the vertical dimension of the particle and hence its volume, which in turn is used to calculate the rain rate from the volume flux per unit time. To confirm the accuracy of the volume flux measurements, Figs. 6a and 6b compare the rain accumulations from the 2DVD and the collocated Geonor rain gauge measurements, for the 4-h time periods for events 1 and 2. For clarity, measurements from only one of the 2DVD instruments are compared. As seen, the agreement with Geonor is excellent in both cases. However, it should be noted that the Geonor gage datalogger's internal time stamp was found to be biased relative to the 2DVD units, which were time stamped via an external time server. The Geonor time profile of accumulation (only available as 10-min accumulations) curves in Fig. 6b as well as Fig. 6a have been shifted by 10 min to align the fast rise in accumulations between the two instruments as far as possible. Even so, if the fall velocity measurements from the 2DVD were not accurate, the drop vertical dimensions would have been in error, and hence the resulting drop volume. The agreement with the Geonor rain gauge in terms of the rain accumulations show there is no systematic error in the fall speed and the related drop volume. Figure 6c compares the 30-min rain accumulations (as a bar graph) from the two 2DVD units and the Geonor rain gauge. During the 30-min period between 0330 and 0400 UTC, the accumulations were 11 and 9 mm for the low-profile and compact 2DVDs as compared with 10.1 mm from the Geonor gage. These comparisons are as close as those reported in Duchon (2008).

Because the images from the two orthogonally placed cameras are obtained from a sequence of line scans, the images often appear skewed when the drop has finite horizontal component of velocity and/or if the drop is canted. As long as the drop possesses an axis of symmetry, the deskewing algorithm described in Schönhuber et al. (2000) and elaborated in Huang et al. (2008) provides for restoration of the images in the two views, as well as an estimation of the canting angles (departure of the symmetry axis from the vertical direction) in the two restored images. The deskewing algorithm was shown to work effectively for drops (>2 mm) for data collected from the 80-m fall bridge experiment reported on by Huang et al. (2008). Moreover, the symmetry of the axis ratio distributions (about the equilibrium value) implied that the dominant mode of oscillation was the axisymmetric (2,0) mode (spherical harmonic $n = 2$, $m = 0$). Such was the case even for the Enhanced Fujita scale 2 (EF2) tornadic event, which occurred on 21 January 2010 in Huntsville, as reported in Thurai et al. (2010), which showed fall speeds close to the GK curve and drop shapes that were similar to those from the 80-m fall experiment.

For the first precipitation event, it was determined that 95% of the 3-mm-sized drop images could be successfully deskewed, whereas for the second event it was considerably lower. In particular, during the 10-min period that showed large fall speed fluctuations (0330–0340 UTC, see Fig. 4) only 60%–70% of the images could be successfully deskewed. It may be inferred that

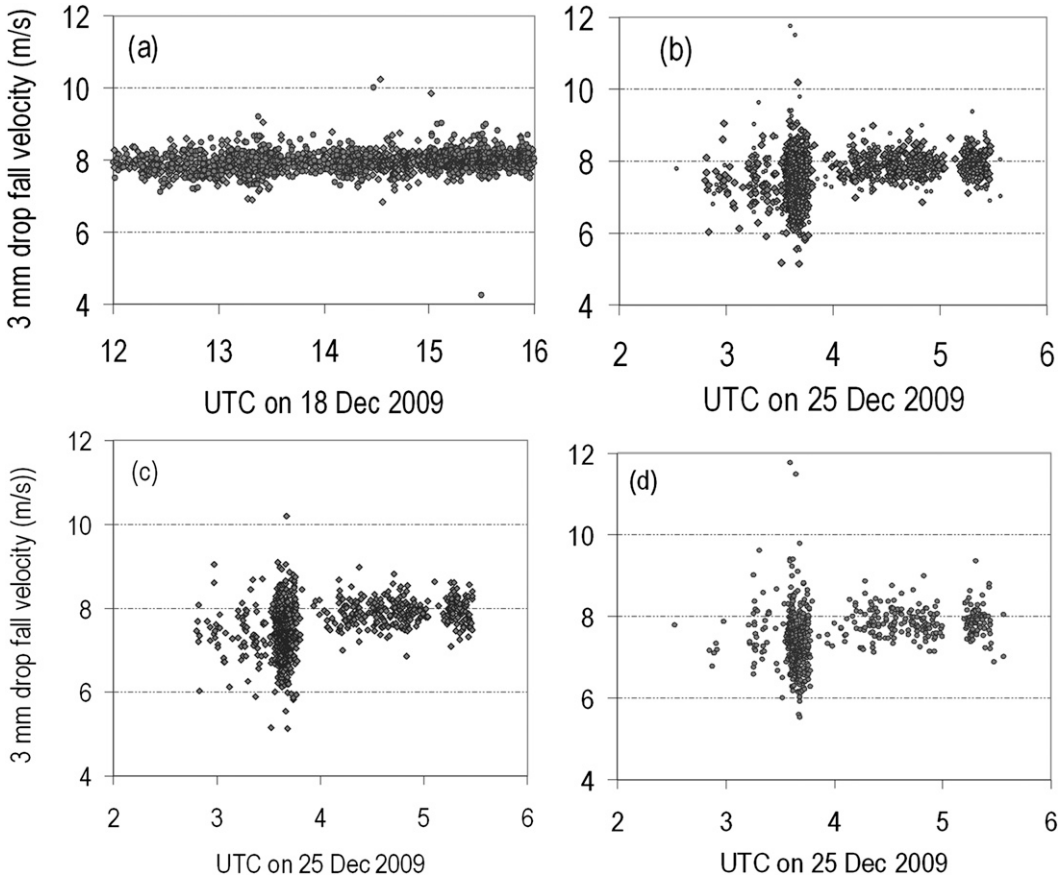

FIG. 4. The measured fall velocity of each individual 3-mm drop as time series (a) for event 1 from both instruments, (b) for event 2 from both instruments, (c) for event 2 from the low-profile 2DVD, and (d) for event 2 from the compact 2DVD. The fall-speed measurement error for this diameter is $\pm 0.08\,\mathrm{m\,s^{-1}}$ (see Table 2 of Schönhuber et al. 2008).

30%–40% of the images could not be deskewed by the algorithm probably because the drops did not possess an axis of symmetry.[2] The main implication here is that these drops are unlikely to be undergoing the normally observed axisymmetric (2, 0) oscillation mode alone. Table 2 shows the percentage of "nondeskewable" drops for various drop diameter intervals for the period 0330–0340 UTC for event 2. The percentage seems to increase with diameter for D_{eq} up to 3 mm and remains somewhat the same for D_{eq} up to 4.5 mm; beyond this, a small decrease can be seen.

Wind effects such as shear-induced turbulence at the surface (assumed isotropic) cause rms canting angles with mean close to 0 and $\sigma < 5°$ as shown theoretically by Beard and Jameson (1983). There is no indication that turbulence would induce sustained drop oscillations. Further, the histograms of drop fall velocities, when compared for cases when the 10-m wind speeds exceeded $7\,\mathrm{m\,s^{-1}}$ and cases for when less than $7\,\mathrm{m\,s^{-1}}$, showed no apparent bias nor any systematic differences, confirming no correlation of drop fall speeds with the 10-m wind speeds.

It was also possible to exclude other hydrometeors (such as low density graupel and other partially melted hydrometeors) by comparing the fall speed distributions separately for the deskewable and nondeskewable particle images. If the negative skewness in the fall speeds is caused by such particles, it would have resulted in different fall speed distributions between the deskewable and nondeskewable cases.

4. Radar observations for event 2

The composite image in Fig. 1b shows that event 2 had an embedded convective line passing over the 2DVD

[2] Note, however, that the volume and fall speed measurements are not affected by the "nondeskewability" of the drop images.

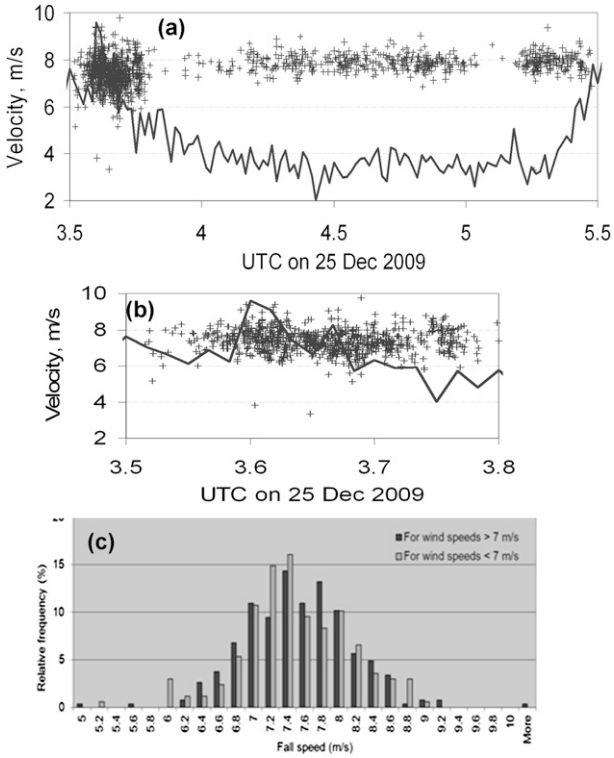

FIG. 5. (a) Time series of 3-mm drop fall velocity (plus signs) and wind velocity (curve) at 10-m height for the 25 Dec 2009 event; (b) as in (a), but zoomed in to cover the time period of the line passage. (c) Histograms of the 3-mm fall speeds for wind speeds > and < 7 m s^{-1}. Note also that the wind speed at 30–40 cm above ground level (the height of the 2DVD sensor area) will be much lower than the wind speeds at 10-m height.

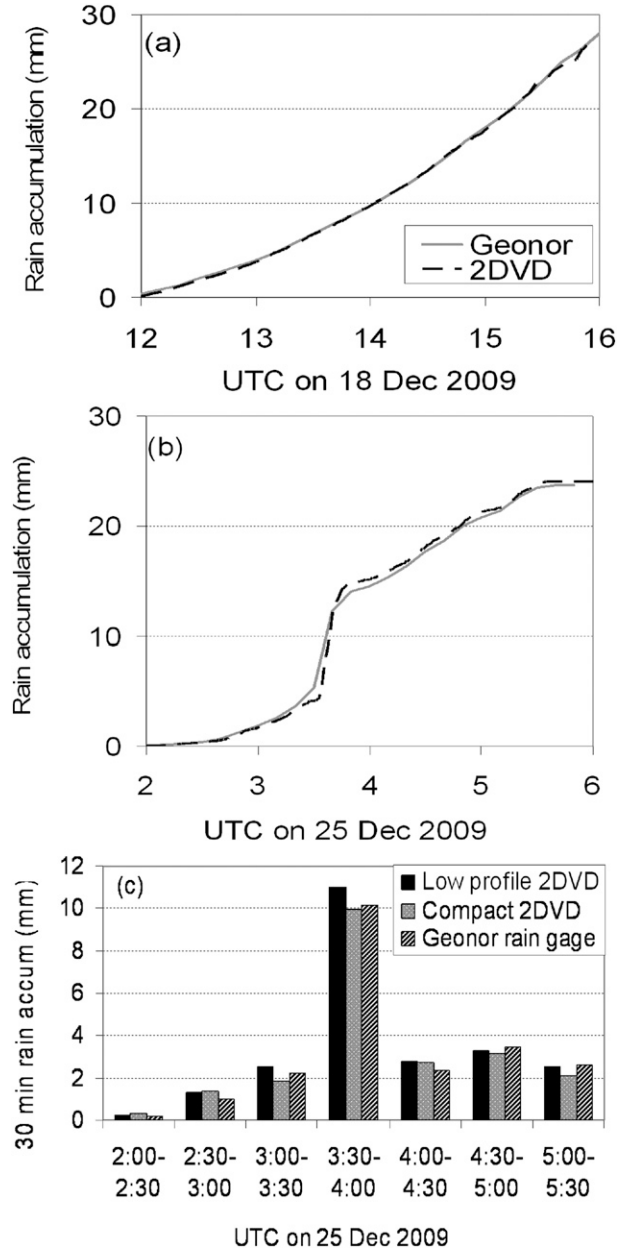

FIG. 6. Comparisons of rain accumulations from the Geonor rain gauge and the low-profile 2DVD for a 4-h period for (a) event 1 and (b) event 2. (c) The 30-min accumulations for event 2.

site. The nearby C-band polarimetric radar, ARMOR, made routine observations during this event consisting of a sequence of plan position indicator (PPI) scans. Figure 7 shows a set of panels of 1.3° elevation PPI scans taken at 0305, 0340, and 0355 UTC. The first column shows Z_h (attenuation corrected), the second column shows Z_{dr} (also attenuation corrected), and the last column shows K_{dp}. The processing and the attenuation-correction procedures used here are very similar to those described in Bringi et al. (2011). The Z_{dr} is corrected using the method described by Tan et al. (1995), which is a gate-by-gate correction method based on a nonlinear relation between the differential attenuation A_{dp} and K_{dp}. Because of the presence of large drops observed with the 2DVD, a ''tuned'' A_{dp}–K_{dp} relation that is based on the disdrometer DSD data was used for correcting Z_{dr} due to differential attenuation. For our ''reference'' drop shapes, this gave rise to $A_{dp} = 0.009K_{dp}^{1.71}$, which is based on a fitted equation for $K_{dp} > 0.7°\,\mathrm{km}^{-1}$. Note the exponent is unusually large relative to the values reported in the literature.

At 0305 UTC, the embedded convective line is seen to the west of the radar. High K_{dp} values are seen in the middle of the convective line. This line moves from southwest to northeast, and at 0340 UTC the line can be seen to lie directly over the 2DVD site, marked with a black asterisk. It is around this time that the 2DVD measurements (Figs. 4c,d) show the larger fall speed

TABLE 2. Percentage of drops with no rotational symmetry axis for event 2 between 0330 and 0340 UTC.

D_{eq} range (mm)	No. of drops	Percent of nondeskewable drop images
1.5–1.75	1553	16
1.75–2.0	1297	18
2.0–2.25	997	23
2.25–2.5	728	28
2.5–2.75	575	30
2.75–3.0	396	29
3.0–3.25	329	35
3.25–3.5	275	31
3.5–3.75	194	31
3.75–4.0	135	32
4.0–4.25	92	30
4.25–4.5	55	31
4.5–4.75	40	25
4.75–5.0	31	28
5.0–5.25	17	24

fluctuations resulting in "slower" speeds and the skewed distribution in Fig. 3. At 0355 UTC, the line moves farther to the northeast and is seen to be fragmenting and/or decaying. At 0305 UTC, that is, when the line was well defined and well organized, the Z_{dr} correction procedure fails to correct for the total differential attenuation beyond the convective line, even when using the aforementioned A_{dp}–K_{dp} relation. At 0340 UTC, there still remains the differential attenuation correction problem beyond the line convection. At 0355 UTC, when the line begins to disintegrate, it becomes possible to restore Z_{dr} consistent with the Z_h values in light rain.

Values of hail signal H_{DR} (Aydin et al. 1986) were computed within the line convection and the upper bound was found to be close to 0 dB with significant numbers of pixels with $H_{DR} < -10$ dB. This largely eliminates the probability of moderate-to-large-sized hail ($D > 1$ cm) (see Bringi and Chandrasekar 2001). The high K_{dp} values within the convective line certainly indicate that heavy rain is the dominant component of the precipitation.

Since the ARMOR operates in the simultaneous transmit and receive mode, one needs to consider bias errors in Z_{dr} due to cross coupling mainly by the antenna in our case (Zrnić et al. 2010; Hubbert et al. 2010a,b). It is reasonable to assume that the newer ARMOR antenna has peak off-axis cross-polarization levels of −30 dB or lower with the lobes occurring symmetrically in the 45°–135° planes. In such a case, Zrnić et al. (2010) estimate the worst-case bias error in Z_{dr} to be <0.1 dB.

On the other hand, from Fig. 12 of Hubbert et al. (2010a), and for a conservative linear depolarization ratio system limit of −30 dB for ARMOR, the magnitude of the bias error is expected to be <0.25 dB at φ_{dp} of 90° (and for slant 45° linear transmit) and <0.6 dB for circular polarization transmit at $\varphi_{dp} = 0$. We note that Hubbert et al. do not account for phase of the cross-polar lobes being 180° out of phase with each other (four-lobe model).

Another possible error source is due to beam blockage, which was determined to be negligible from the occultation map at the 1.3° elevation angle for the observed refractive conditions on 25 December 2009 at 0300 UTC. Additionally, the rain-accumulation map for this entire event, even with a simple Z–R relation did not show any artifacts due to clutter.

The radial velocity plots associated with this event are shown in Fig. 8, taken from the 1.3° elevation PPI scans at 0305 UTC (left panel) and 0340 UTC (right panel). In both cases, a narrow convergence zone at the leading edge of the convective line is present (dash–dotted line). At 0305 UTC, the thin line of radial convergence is apparent west of the radar as well as the 2DVD site (marked with a plus sign). This narrow zone of convergence marks the outflow boundary produced by the convective line. At 0340 UTC, 35 min later, the outflow boundary has moved east of the 2DVD site while the core of the convective line is positioned directly over the 2DVD site. Between the core of the convective line and its outflow boundary, at 0340 UTC is a small region near the 2DVD site (enclosed by the box) consisting of both radial divergent and convergent signatures, which are associated with the wavelike features present behind outflow boundaries (Wakimoto 1982). Since the elevation angle of the ARMOR scan was only 1.3°, the horizontal motions within the convective line contribute largely to the measured radial velocity patterns around the 2DVD site at 0340 UTC.

Temperature recordings at ground level at the 2DVD site showed a decrease from 12° to 10°C during passage of the convective line. The height of the melting level was estimated to be around 2 km, based on the 2° elevation PPI scans of the copolar correlation coefficient (not shown here). The 0000 UTC soundings showed the 0°C height of around 3.0 km. The pressure at 2 m MSL ranged from 1005 to 1003 hPa during the passage of the embedded line convection.

5. Discussion of combined radar and 2DVD results

Thus far, we have observed the following with respect to the second event:

- At around 0340 UTC, the 2DVD measurements show significant negative skewness (toward slower speeds)

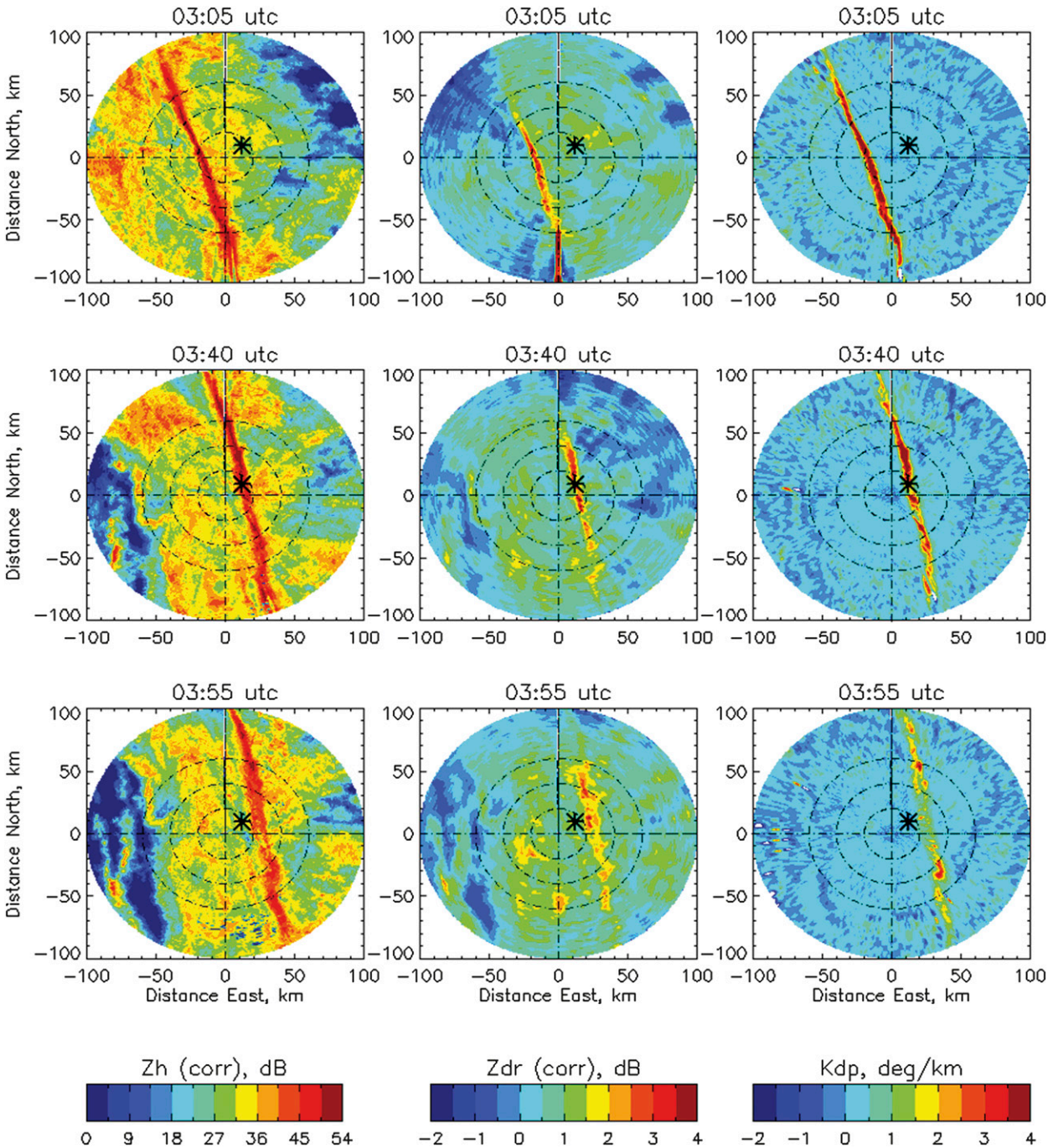

FIG. 7. PPI scans of (left) attenuation-corrected Z_h, (middle) attenuation-corrected Z_{dr}, and (right) K_{dp}, taken at (top to bottom) 0305, 0340, and 0355 UTC. The 2DVD site is marked with an asterisk sign along azimuth 52° and range 15 km.

in the fall speed distributions (e.g., for the 3-mm and larger drops).

- A large fraction of these drops are inferred to have shapes without an axis of rotational symmetry.
- Radar PPI scans show an organized narrow line convection crossing the 2DVD site at this time, with a convergence zone ahead of the line.
- Large Z_{dr} and higher-than-expected differential attenuation (between H and V polarizations) within the line convection.

The above can be potentially explained if we assume that the drops—within the line convection—are undergoing mixed-mode oscillations (axisymmetric plus

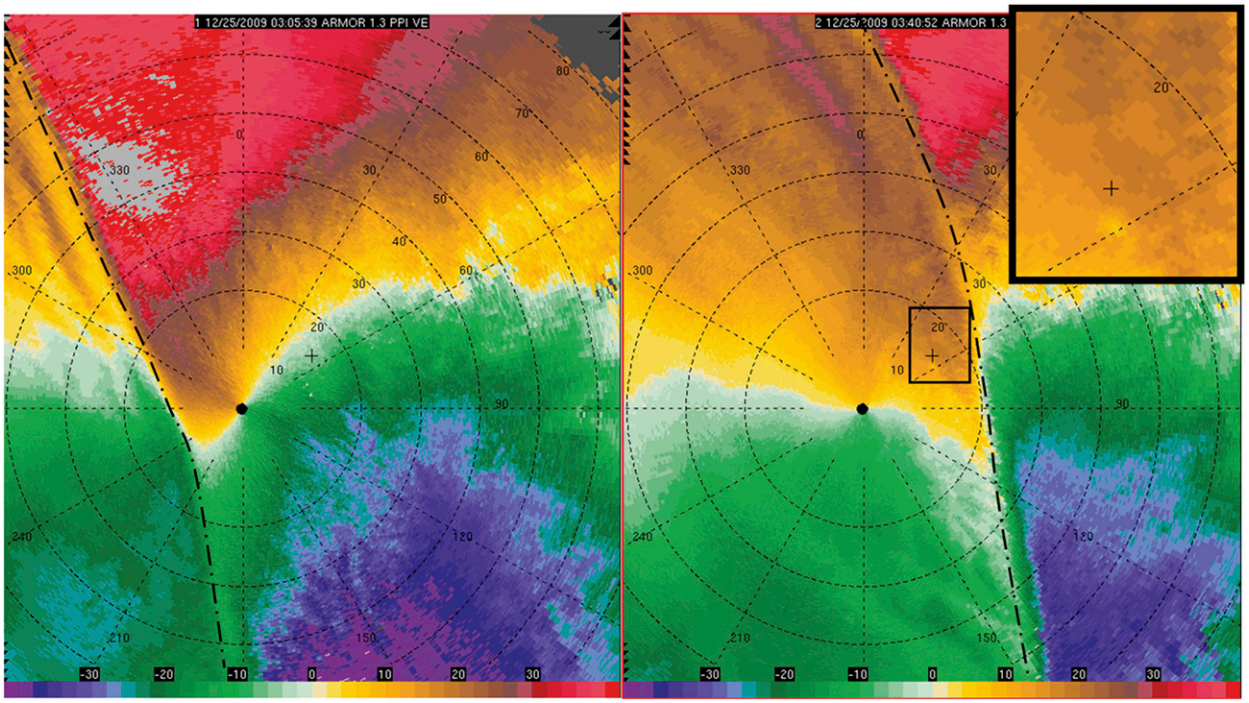

FIG. 8. Radial velocity (m s^{-1}) measured by ARMOR at an elevation of 1.3° at (left) 0305 and (right) 0340 UTC 25 Dec 2009. A narrow convergence zone at the leading edge of the convection line is present (dash–dotted line) near the 2DVD site (plus sign; right panel). The inset picture in the right panel is an enlarged image of the radial velocity in the region enclosed by the box in the right panel.

horizontal oscillation modes). Mixed-mode oscillations have been observed in several wind-tunnel studies. Some early examples are Blanchard (1950), Brook and Latham (1968), and Nelson and Gokhale (1972). Additionally, Goodall (1976) conducted a microwave scattering study (both horizontally and vertically polarized) of drop oscillations in a wind tunnel and found strong evidence of horizontal-mode oscillations. Feng and Beard (1991) developed a perturbation model for determining the oscillation mode frequencies and compared their model predictions with the previous wind-tunnel data (see their Fig. 7). Further, based on Fig. 13 of Beard et al. (2010), it would seem that the energy required to maintain horizontal-mode oscillations (against viscous dissipation) is much lower than for the transverse mode (for $D < 2$ mm). It is reasonable to expect the same tendency to hold for larger-sized drops.

The 2DVD images of the drops can be considered to be instantaneous "snapshots" because the line scan camera speed is much higher than the drop oscillation frequency. It is therefore possible to extend our estimates (quoted in the last two paragraphs of section 3) of the percentage of drops without a rotational symmetry axis to a percentage of time that a given drop "spends" in the horizontal oscillation mode. For the first event, this percentage was low (around 5%) throughout the event. For event 2, this percentage is as much as 30%–40% during the passage of the line convection. This percentage of drops was found to be somewhat independent of drop size (see Table 2). Since the horizontal mode possesses no axis of rotational symmetry during its oscillation cycle, the 30%–40% figure strongly suggests that a significant component is due to the horizontal-mode oscillations. If so, one could expect a possible increase in the time-averaged drag force (due to increased effective area presented to the flow), which in turn would explain the negative skewness of the fall velocity distribution. Note that in still air the fall speed response time is approximately 0.5–1 s (from Pruppacher and Klett 1997), which is slower than the drop oscillation frequencies, which are around 10–30 Hz for the horizontal mode [see, e.g., Fig. 11 in Beard et al. (2010) for $D > 3$ mm]. However, as Pruppacher and Klett (1997) indicate, "If a drop is deformed, the drag and thus the terminal velocity are functions also of the amount of the drop's deformation."

One method of sustaining horizontal-mode oscillations is drop collisions in moderate-to-intense rain rates. Beard and Johnson (1984) have modeled the effects of such collisional forcing on the average axis ratios and found that the horizontal mode does indeed give rise to more oblateness as compared with axisymmetric mode, especially for rain rates > 30 mm h^{-1}. The effect on Z_{dr} was also computed and shown to have a significant

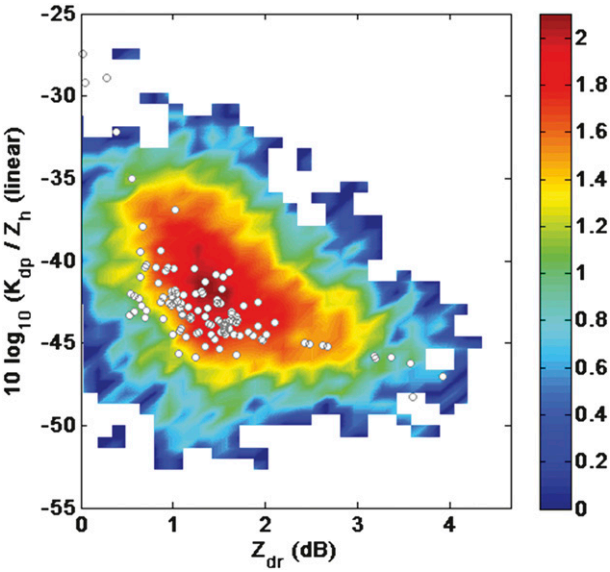

FIG. 9. Frequency of occurrence of the quantity $10\log_{10}(K_{dp}/Z_h)$ as a function of Z_{dr} for the second event extracted from the C-band radar data within the line convection region. For comparison, simulations based on the measured 1-min drop size distributions are shown as white points using our standard drop shape model [given in Eqs. (1) and (2) in Thurai et al. 2007]. Gaussian noise has been added to both sets of scattering simulations.

increase for horizontal mode as opposed to the axisymmetric mode. It follows that the inference of relatively frequent horizontal-mode oscillations from the 2DVD data during the passage of the convection line in event 2 should be reflected in the polarimetric radar measurements. To verify whether this is the case, we adopt the procedure described in Gorgucci et al. (2006). The method uses the variation of $\chi = 10\log_{10}(Z_h^{\mathrm{linear}}/K_{dp})$ with Z_{dr} to assess the "effective" drop axis ratios from the radar measurements, where Z_h^{linear} is Z_h in linear units. The advantage of this method is that the term χ is somewhat independent of the drop size distribution. However, for the method to be applicable, both Z_h and Z_{dr} need to be very accurately calibrated, and furthermore, proper attenuation correction procedures must also be applied. In our case, the calibration of Z_h and Z_{dr} were established by comparing the radar data extracted over the disdrometer site with corresponding 2DVD measurements collected well after the line of convection had passed over the 2DVD site, that is, between 0400 and 0500 UTC. The calibration factors were found to be relatively steady throughout the hour for both Z_h and Z_{dr}. (The PPI scans given in earlier Fig. 7 represent radar data after applying the calibrations as well as attenuation corrections.)

Figure 9 shows the variation of χ with Z_{dr} determined for the 0340 PPI scan data, taken only within the line convection region (since the above mentioned A_{dp}–K_{dp} relation failed to adequately correct for differential attenuation beyond the line). Superimposed (as white dots) are the scattering calculations using the measured drop size distributions from the two collocated disdrometers and the drop shape model given in Thurai et al. (2007). To simulate the noise in radar measurements, we have added Gaussian noises to Z_{dr} and K_{dp} with standard deviations of 0.2 dB and 0.1° km^{-1}, respectively. As seen, the simulation points do not traverse the most probable variation and in fact lie toward the lower Z_{dr} direction; that is, the measured Z_{dr} is higher than the expected values if one assumes the above drop shape model. The presence of more oblate drops (on a time-averaged basis) is indicated, which is also with what the 2DVD measurements had indicated earlier (albeit at ground level); that is, 30%–40% of the drops were undergoing mixed-mode oscillations.

Additional evidence for mixed-mode oscillations was also provided by the copolar correlation coefficient ρ_{hv} data (not shown here). The scattering calculations mentioned earlier had resulted in expected ρ_{hv} values as low as 0.95 (which includes non-Rayleigh effects). The low values arise because of the wide DSDs with large drops, which in turn will result in wide axis ratio distributions. This was shown in a case study (Thurai et al. 2008) in Ontario that clearly indicated a ρ_{hv} dip at C band when wide DSDs were recorded by a 2DVD. The calculated ρ_{hv} dip was consistent with the radar measurements for that case. However, for the event relating to Fig. 9, ρ_{hv} dips were considerably lower than the expected values; that is, instead of 0.95, the radar data showed values down to 0.8 (and occasionally even lower) within the line convection. Such low values are consistent with the notion of mixed-mode oscillations.

The fundamental drop oscillation modes are always present [as shown by Szakáll et al. (2010) from wind-tunnel measurements], but under normal atmospheric conditions, the (2, 0) mode dominates. The 2DVD measurements of drop shapes in numerous locations have also shown this to be the case. The most probable explanation for event 2 reported in this paper is sustained drop collisions within the convection line, which causes the other two modes to increase in amplitudes. High-speed video imaging of drop collisions between a ~3-mm drop and a much smaller drop (the most probable collision scenario) conducted using the wind-tunnel facility has already revealed that the larger drops exhibit transient shapes upon collision that last at least for 0.3 s, for both coalescence and noncoalescence cases. If collisions occur typically at a rate of 0.2 s^{-1} [for 3-mm drops in a 55-dBZ reflectivity rain column, from Rogers (1989)], then it is conceivable that collisions can sustain

drop oscillations (against viscous dissipation) for a significant fraction of the 3-mm drops. This has also been hypothesized in Jameson and Durden (1996) from airborne measurements of copolar and cross-polar backscatter from tropical storms. For event 2, high rain intensity within the narrow line convection significantly increases the likelihood of drop collisions. Moreover, in the case of rain clustering (see, e.g., Jameson and Kostinski 1999), which may well be the case within the embedded line convection in event 2, drop collision rates can increase significantly by a factor of up to 3.5 (McFarquhar 2004).

In another study (Aresu et al. 1993), this time relating to propagation effects on terrestrial links using data from a short line-of-sight link at 30 GHz, an event analysis has clearly indicated the presence of "more deformed drops" than normal.

It should be stressed here that this particular event (i.e., event 2 on 25 December 2009) is a somewhat unusual case that was investigated because of the negative skewness in the fall velocity distributions (Fig. 3) from the 2DVD measurements. In many other cases including event 1 on 18 December 2009 and the EF2 tornado event reported in Thurai et al. (2010), no evidence was found to indicate significant mixed-mode drop oscillations or lower fall speeds. In fact, the tornado event had higher wind speeds than those associated with event 2 reported here. Since we have two collocated 2DVDs, the confidence in our measurements is greatly enhanced (provided there is agreement between the two). Such data, together with simultaneous ARMOR observations, will form part of an ongoing study to identify cases where significant deviations from mean shapes and the expected fall velocities of raindrops seem to occur.

6. Summary

Two rain events that occurred 7 days apart in Huntsville, Alabama, have been investigated using two collocated 2DVDs, as well as simultaneous observations from the ARMOR C-band polarimetric radar. For each event, drop fall speeds and shapes were examined from the 2DVD measurements, with specific focus placed on 3-mm diameter drops. The first event—on 18 December 2009—showed a narrow distribution of fall velocities that follow the Atlas et al. (1973) expected curve; for example, the 3-mm drops had velocities that were symmetrically distributed, with a mode at around 7.9–8 m s^{-1}. The second event—on 25 December 2009—showed a negatively skewed fall speed distribution, with a significant number of drops having lower-than-expected fall speeds. The 25 December event had a highly organized, narrow, embedded line of convection that fortuitously traversed the 2DVD site. Time series of the 3-mm drop fall velocity measurements showed that these "slow" drops were detected only during passage of this line. The digitized images of the drops were also examined. It was inferred that around 30%–40% of the drops did not have an axis of rotational symmetry, which directly implies that the drops are undergoing asymmetric oscillations (mainly horizontal mode) for a significant fraction of the time. The corresponding fraction for the first event was only 5%, which indicates the dominant drop oscillation mode to be the (2, 0) axisymmetric mode. Our inference regarding the second event is that the slower fall speeds may have resulted from increased drag caused by asymmetric horizontal-mode oscillations.

Supporting this inference, simultaneous radar observations from the C-band ARMOR were also analyzed for the second event. The self-consistency among Z_h, Z_{dr}, and K_{dp} was tested for two different drop shape models, including our standard shapes from the 80-m fall experiment. The results show that more oblate drop shapes, which can be enhanced because of mixed mode, including the horizontal-mode oscillations, are needed to explain the radar-based variation of (K_{dp}/Z_h) versus Z_{dr}. Note also that asymmetric oscillations can cause signal depolarization.

Studies are ongoing to identify other cases that show significant deviations from mean shapes and the expected fall velocities, observed from both 2DVDs, accompanied by the C-band polarimetric radar observations. We will use these additional cases to examine the potential associations among the high wind speed environment within a convective line, rain drop oscillations, and fall speed deviations.

Acknowledgments. The work is primarily supported by the National Science Foundation via Grant AGS-0924622. Support from Dr. Ramesh Kakar, NASA Precipitation Measurement Mission (PMM), NASA Grant Award NNX10AJ12G, and the Global Precipitation Measurement Mission Flight Project, is also acknowledged. The authors also thank Dr. Ali Tokay and Dr. Larry Carey for helpful discussions.

REFERENCES

Aresu, A., A. Martellucci, and A. Paraboni, 1993: Experimental assessment of rain anisotropy and canting angle in a horizontal path at 30 GHz. *IEEE Trans. Antennas Propag.,* **41,** 1331–1335.

Atlas, D., R. C. Srivastava, and R. S. Sekhon, 1973: Doppler radar characteristics of precipitation at vertical incidence. *Rev. Geophys.,* **11,** 1–35.

Aydin, K., T. A. Seliga, and V. Balaji, 1986: Remote sensing of hail with a dual linear polarization radar. *J. Climate Appl. Meteor.,* **25,** 1475–1484.

Barthazy, E., S. Göke, R. Schefold, and D. Högl, 2004: An optical array instrument for shape and fall velocity measurements of hydrometeors. *J. Atmos. Oceanic Technol.,* **21,** 1400–1416.

Beard, K. V., 1984: Oscillation modes for predicting raindrop axis and back scatter ratios. *Radio Sci.,* **19,** 67–74.

——, and A. R. Jameson, 1983: Raindrop canting. *J. Atmos. Sci.,* **40,** 448–454.

——, and D. B. Johnson, 1984: Raindrop axial and backscatter ratios using a collisional probability model. *Geophys. Res. Lett.,* **11,** 65–68.

——, and C. Chuang, 1987: A new model for the equilibrium shape of raindrops. *J. Atmos. Sci.,* **44,** 1509–1524.

——, and R. J. Kubesh, 1991: Laboratory measurements of small raindrop distortion. Part II: Oscillation frequencies and modes. *J. Atmos. Sci.,* **48,** 2245–2264.

——, V. N. Bringi, and M. Thurai, 2010: A new understanding of raindrop shape. *Atmos. Res.,* **97,** 396–415.

Blanchard, D. C., 1950: The behavior of water drops at terminal velocity in air. *Trans. Amer. Geophys. Union.,* **31,** 836–842.

Brandes, E. A., G. Zhang, and J. Vivekanandan, 2002: Experiments in rainfall estimation with a polarimetric radar in a subtropical environment. *J. Appl. Meteor.,* **41,** 674–684.

Bringi, V. N., and V. Chandrasekar, 2001: *Polarimetric Doppler Weather Radar: Principles and Applications.* Cambridge University Press, 636 pp.

——, M. A. Rico-Ramirez, and M. Thurai, 2011: Rainfall estimation with an operational polarimetric C-band radar in the United Kingdom: Comparison with a gauge network and error analysis. *J. Hydrometeor.,* **12,** 935–954.

Brook, M., and D. J. Latham, 1968: Fluctuating radar echo: Modulation by vibrating drops. *J. Geophys. Res.,* **73,** 7137–7144.

Duchon, C., 2008: Vibrating wire technology for precipitation measurements. *Precipitation: Advances in Measurement, Estimation and Prediction,* S. Michaelides, Ed., Springer, 33–58.

Feng, J. Q., and K. V. Beard, 1991: A perturbation model of raindrop oscillation characteristics with aerodynamic effects. *J. Atmos. Sci.,* **48,** 1856–1868.

Foote, G. B., 1973: A numerical method for studying liquid drop behavior: Simple oscillation. *J. Comput. Phys.,* **11,** 417–435.

Godfrey, C. M., 2002: A scheme for correcting rainfall rates measured by a 2-D video disdrometer. M.Sc. thesis, School of Meteorology, University of Oklahoma, 119 pp.

Goodall, F., 1976: Propagation through distorted water drops at 11 GHz. Ph.D. dissertation, University of Bradford, 205 pp.

Gorgucci, E., L. Baldini, and V. Chandrasekar, 2006: What is the shape of a raindrop? An answer from radar measurements. *J. Atmos. Sci.,* **63,** 3033–3044.

Gunn, K. L. S., and G. D. Kinzer, 1949: The terminal velocity of fall for water droplets in stagnant air. *J. Meteor.,* **6,** 243–248.

Hobbs, P. V., J. D. Locatelli, and J. E. Martin, 1996: A new conceptual model for cyclones generated in the lee of the Rocky Mountains. *Bull. Amer. Meteor. Soc.,* **77,** 1169–1178.

Huang, G.-J., V. N. Bringi, and M. Thurai, 2008: Orientation angle distributions of drops after an 80-m fall using a 2D video disdrometer. *J. Atmos. Oceanic Technol.,* **25,** 1717–1723.

——, ——, R. Cifelli, D. Hudak, and W. A. Petersen, 2010: A methodology to derive radar reflectivity–liquid equivalent snow rate relations using C-band radar and a 2D video disdrometer. *J. Atmos. Oceanic Technol.,* **27,** 637–651.

Hubbert, J. C., S. M. Ellis, M. Dixon, and G. Meymaris, 2010a: Modeling, error analysis, and evaluation of dual-polarization variables obtained from simultaneous horizontal and vertical polarization transmit radar. Part I: Modeling and antenna errors. *J. Atmos. Oceanic Technol.,* **27,** 1583–1598.

——, ——, ——, and ——, 2010b: Modeling, error analysis, and evaluation of dual-polarization variables obtained from simultaneous horizontal and vertical polarization transmit radar. Part II: Experimental data. *J. Atmos. Oceanic Technol.,* **27,** 1599–1607.

Jameson, A. R., and S. L. Durden, 1996: A possible origin of linear depolarization observed at vertical incidence in rain. *J. Appl. Meteor.,* **35,** 271–277.

——, and A. B. Kostinski, 1999: Fluctuation properties of precipitation. Part V: Distribution of rain rates—Theory and observations in clustered rain. *J. Atmos. Sci.,* **56,** 3920–3932.

Kubesh, R. J., and K. V. Beard, 1993: Laboratory measurements of spontaneous oscillations for moderate-size raindrops. *J. Atmos. Sci.,* **50,** 1089–1098.

Löffler-Mang, M., and J. Joss, 2000: An optical disdrometer for measuring size and velocity of hydrometeors. *J. Atmos. Oceanic Technol.,* **17,** 130–139.

McFarquhar, G. M., 2004: The effect of raindrop clustering on collision-induced break-up of raindrops. *Quart. J. Roy. Meteor. Soc.,* **130,** 2169–2190.

Montero-Martinez, G., A. B. Kostinski, R. A. Shaw, and F. Garcia-Garcia, 2009: Do all raindrops fall at terminal speed? *Geophys. Res. Lett.,* **36,** L11818, doi:10.1029/2008GL037111.

Nelson, A. R., and N. R. Gokhale, 1972: Oscillation frequencies of freely suspended water drops. *J. Geophys. Res.,* **77,** 2724–2727.

Nešpor, V., W. F. Krajewski, and A. Kruger, 2000: Wind-induced error of raindrop size distribution measurement using a two-dimensional video disdrometer. *J. Atmos. Oceanic Technol.,* **17,** 1483–1492.

Petersen, W. A., K. R. Knupp, D. J. Cecil, and J. R. Mecikalski, 2007: The University of Alabama Huntsville THOR Center instrumentation: Research and operational collaboration, Preprints, *33rd Int. Conf. on Radar Meteorology,* Cairns, Australia, Amer. Meteor. Soc., 5.1. [Available online at https://ams.confex.com/ams/33Radar/webprogram/Paper123410.html.]

Pruppacher, H. R., and K. V. Klett, 1997: *Microphysics of Clouds and Precipitation.* 2nd ed. Kluwer Academic Publishers, 954 pp.

Rogers, R. R., 1989: Raindrop collision rates. *J. Atmos. Sci.,* **46,** 2469–2472.

Schönhuber, M., W. L. Randeu, H. E. Urban, and J. P. V. Poiares Baptista, 2000: Field measurements of raindrop orientation angles. *Proc. AP2000 Millennium Conf. on Antennas and Propagation,* Davos, Switzerland, ESA, paper 1017. [Available online at http://distrometer.at/pdf/P1017.pdf.]

——, G. Lammer, and W. L. Randeu, 2008: The 2D-video-distrometer. *Precipitation: Advances in Measurement, Estimation and Prediction,* S. Michaelides, Ed., Springer, 3–32.

Schuur, T. J., A. V. Ryzhkov, D. S. Zrnić, and M. Schönhuber, 2001: Drop size distributions measured by a 2D video disdrometer: Comparison with dual-polarization radar data. *J. Appl. Meteor.,* **40,** 1019–1034.

Szakáll, M., K. Diehl, S. K. Mitra, and S. Borrmann, 2009: A wind tunnel study on the shape, oscillation, and internal circulation of large raindrops with sizes between 2.5 and 7.5 mm. *J. Atmos. Sci.,* **66,** 755–765.

——, ——, ——, and ——, 2010: Shapes and oscillations of falling raindrops—A review. *Atmos. Res.,* **97,** 416–425.

Tan, J., J. W. F. Goddard, and M. Thurai, 1995: Applications of differential propagation phase in polarization-diversity radars at S-band and C-band. *Proc. Ninth Int. Conf. on Antennas and*

Propagation, Eindhoven, Netherlands, IET Conf. Publ. 407 (2), 336–341.

Testik, F. Y., A. P. Barros, and L. F. Bliven, 2006: Field observations of multimode raindrop oscillations by high-speed imaging. *J. Atmos. Sci.,* **63,** 2663–2668.

Thurai, M., and V. N. Bringi, 2005: Drop axis ratios from a 2D video disdrometer. *J. Atmos. Oceanic Technol.,* **22,** 966–978.

——, G. J. Huang, V. N. Bringi, W. L. Randeu, and M. Schönhuber, 2007: Drop shapes, model comparisons, and calculations of polarimetric radar parameters in rain. *J. Atmos. Oceanic Technol.,* **24,** 1019–1032.

——, D. Hudak, and V. N. Bringi, 2008: On the possible use of copolar correlation coefficient for improving the drop size distribution estimates at C band. *J. Atmos. Oceanic Technol.,* **25,** 1873–1880.

——, V. N. Bringi, and W. A. Petersen, 2009a: Rain microstructure retrievals using 2-D video disdrometer and C-band polarimetric radar. *Adv. Geosci.,* **20,** 13–18.

——, ——, M. Szakáll, S. K. Mitra, K. V. Beard, and S. Borrmann, 2009b: Drop shapes and axis ratio distributions: Comparison between 2D video disdrometer and wind-tunnel measurements. *J. Atmos. Oceanic Technol.,* **26,** 1427–1432.

——, W. A. Petersen, and L. D. Carey, 2010: DSD characteristics of a cool-season tornadic storm using C-band polarimetric radar and two 2D-video disdrometers. *Extended abstracts, ERAD 2010—The Sixth European Conf. on Radar in Meteorology and Hydrology,* Sibiu, Romania. [Available online at http://www.erad2010.org/pdf/oral/tuesday/radpol1/5_ERAD2010_0101.pdf.]

Tokay, A., and K. V. Beard, 1996: A field study of raindrop oscillations. Part I: Observation of size spectra and evaluation of oscillation causes. *J. Appl. Meteor.,* **35,** 1671–1687.

Wakimoto, R. M., 1982: The life cycle of thunderstorm gust fronts as viewed with Doppler radar and rawinsonde data. *Mon. Wea. Rev.,* **110,** 1060–1082.

Zrnić, D., R. Doviak, G. Zhang, and A. Ryzhkov, 2010: Bias in differential reflectivity due to cross coupling through the radiation patterns of polarimetric weather radars. *J. Atmos. Oceanic Technol.,* **27,** 1624–1637.